JOURNAL OF MATERIALS SCIENCE 30 (1995) 2220–2226

A study of nanocrystalline iron and aluminium metals and Fe_3Al intermetallic by mechanical alloying

E. BONETTI, G. SCIPIONE, G. VALDRÈ
Dipartimento di Fisica, via Irnerio 46, I-40126 Bologna, Italy
S. ENZO, R. FRATTINI, P. P. MACRÌ
Dipartimento di Chimica Fisica, D. D. 2137, I-30123 Venezia, Italy

Pure iron and aluminium powders and a mixture of composition $Fe_{75}Al_{25}$ were treated mechanically in a high-energy mill for up to 40 h. X-ray diffraction and analytical transmission electron microscopy were coupled to elastic energy dissipation and dynamic Young's modulus measurements to study the structural transformation of the specimens induced by the mechanical treatment. A quantitative comparison between the structural behaviour of the pure elements and of the mixture was carried out. The role of the parameters such as the composition, the grain size and the activation energy during the process was examined in relation to the competing mechanisms of plastic deformation and recovery.

1. Introduction

At present, the processing of pure metal powders by mechanical alloying (MA) is receiving great attention as an innovative technique for producing amorphous metallic alloys [1–3]. Moreover, a further interest has been supplied by the possibility of preparing mono- and multi-component metallic materials in the size range of a few nanometres [4–6]. One-component single-phase powders of palladium, aluminium, nickel, copper, titanium [7–10], as well as various single-phase intermetallics [11–13], were synthesized by mechanical milling and alloying (MM and MA) as efficient methods to produce very fine metallic powders as alternatives to the methods of sputtering and evaporation of metals. These systems are expected to exhibit new properties due to a high ratio of the surface atoms with respect to the total number of atoms and were characterized using different approaches depending on their source. A "gas-like" phase was reported recently to account for the thermodynamical properties exhibited by highly fragmented and disordered iron particles prepared by MA and MM [14]. This "gas-like" phase was reported earlier [15] for nanocrystals synthesized by the gas-condensation method to account for the high background intensity observed in the X-ray diffraction diagrams. Recently, Wagner and Boldrick [11] analysed the X-ray diffraction data of several nanocrystalline systems, such as iron, platinum, NiAl and Ag–Cu binary compounds, obtained by different methods; these authors denied the existence of a "gas-like" phase, supposed to be an amorphous component. On the other hand, recent studies on the thermodynamical properties of palladium nanoparticles [16, 17] provided a different explanation for the macroscopic behaviour. An "interfacial" phase, with displacement of atoms exceeding 50% of the interatomic distance, can account for an observed increase of the specific heat in palladium and copper nanoparticles [16]. Conversely, the preferred orientation and the Debye–Waller parameter, which differs from the corresponding bulk value, may vary the properties of nanocrystalline palladium particles [17]. In any case, it is expected that the reduction of grain size and the increase of lattice disorder will enhance the chemical reactivity of the powders, as is well known in catalysis.

The structural behaviour of single-component phases such as iron and aluminium has not yet been studied by investigating their solid solutions and intermetallics at the same time. In fact, Morris and Morris [18] and Dong *et al.* [19] studied the Fe–Al system in the aluminium-rich side, whilst Zák *et al.* [20] ball milled (MM method) the Fe_3Al intermetallic. Analogously, Yelsukov *et al.* [21] studied the structure and magnetic properties of Fe–Al alloys synthesized by arc melting and disordered by ball milling in the aluminium concentration range 0–60 at %.

Because the end-products of the MA and MM methods are reported to be highly dependent on the milling machine [22], we investigated the Fe–Al system synthesized by MA in a systematic way. The thermal stability and transformation mechanisms following the milling of elemental powders of pure iron and aluminium and of a mixture with the ratio Fe : Al = 3 : 1 processed by MA, have been compared.

The structural transformations were studied by X-ray diffraction (XRD), transmission electron microscopy (TEM), differential scanning calorimetry (DSC) and high spatial resolution energy dispersive spectroscopy (EDS). In addition, elastic energy dissipation coefficient (internal friction) and dynamic Young's modulus measurements were performed to follow the

0022–2461

details of the transformation process. This approach was intended to quantify thermodynamic properties such as the activation energy of the transformations and to investigate the role of the crystallite size involved in the process from solid solution to intermetallic.

2. Materials and methods

Pure metal powders of aluminium and iron (325 mesh, Alfa Products, 99.9% purity) were milled in a SPEX mixer/mill model 8000 in an argon atmosphere with an oxygen content below 5 p.p.m. The weight of the powders was about 10 g, and the ball-to-powder weight ratio was 8:1.

The consolidation procedure consisted in the cold pressing of about 0.5 g milled powders by means of a specifically constructed die with rectangular section of $15 \times 5\ mm^2$ and a piston under an axial pressure of about 1.5 GPa.

X-ray diffraction measurements were performed with a symmetrical Bragg-Brentano goniometer using CuK_α and CoK_α radiations and a monochromator in the diffracted beam.

A line profile analysis was performed on the wide-angle X-ray scattering (WAXS) spectra of powdered samples using a fitting procedure reported elsewhere [23]. Pseudo-Voigt functions $V(Q)$ were used to describe the α_1–α_2 peak shape according to the following equation

$$V(Q) = I_p[nG(Q - Q_0) + (1 - n)L(Q - Q_0)] \quad (1)$$

where I_p is the peak intensity, n a mixing parameter varying between 0 (totally Lorentzian shape) and 1 (totally Gaussian), Q_0 the peak position

$$G(Q - Q_0) = \exp\{-\ln 2[(Q - Q_0)/w_1 A]^2\} \quad (2)$$

is a Gaussian function, and

$$L(Q - Q_0) = \{1 + [(Q - Q_0)/w_1 A]^2\}^{-1} \quad (3)$$

is a Cauchy (or Lorentzian) function. w_1 is the half-width at half maximum at the low Q side of the diffraction peak and $A = w_l/w_h$ is an asymmetry parameter expressed as the ratio between half width at low and high Q, respectively. Thus each peak has five adjustable parameters, namely I_p, q_0, n, w_l and A, plus two more accounting for a sloping background according to a straight line. Because the area under a pseudo-Voigt peak is analytically known, the integral breadth, β, can be calculated from the adjusted parameters according to the expression

$$\beta = (1 + A)w_l[n(\pi/\ln 2)^{1/2} + (1 - n)\pi]/2 \quad (4)$$

This value is used in the Scherrer equation [24] to calculate a volume weighted average crystallite size, comprehensive of lattice disorder. The integral breadth, β, depends on the root mean square strain, $\langle \varepsilon^2 \rangle^{1/2}$, and on the effective crystallite size, $\langle D \rangle$, according to Wagner [25], as

$$\beta = 2\pi/\langle D \rangle + \langle \varepsilon^2 \rangle^{1/2} Q/2 \quad (5)$$

The value for $\langle D \rangle$ is calculated after extrapolation to $Q = 0$ of the linear behaviour of β_{hkl} versus Q_{hkl}, $h\,k\,l$ being the (1 1 0) and (2 2 0) couple of reflections.

Specimens for TEM were prepared by ultramicrotomy following a method already described [6]. Electron-transparent slices of about 80 nm thick were obtained from a dispersion of the starting powders embedded in epoxidic resin. TEM observations and X-ray EDS analyses were performed with a field-emission gun Philips EM400T transmission electron microscope operating at 100 kV equipped with an EDAX PV 9900 EDS.

Young's modulus and elastic energy dissipation measurements were performed on the cold consolidated powders by the vibrating reed technique. The electrostatic excitation and the frequency modulation detection of the flexural vibration of the thin reed were investigated in the range 500–5000 Hz. The strain amplitude never exceeded 10^{-5} and all measurements, in isochronal conditions, were performed at a constant heating rate of $150\ K\,h^{-1}$.

DSC analyses were carried out with a DSC7 Perkin–Elmer calorimeter. The powders were crimped in aluminium pans and heated at a constant rate of $20\ K\,min^{-1}$ under a flow of purified argon.

3. Results and discussion

Fig. 1a and b show the XRD logarithmic intensity versus the scattering vector Q, respectively, for pure α-iron and pure aluminium milled for the times quoted. The general trend, as a function of the milling time, displays a progressive broadening of the XRD profiles indicative of a crystallite size reduction and/or of an increase of the atomic level strain. However, in agreement with other work [4, 5], no modification of the original crystalline lattices is observed in the pure elements and the peak positions remain constant during the mechanical treatment. This is different from the structural evolution of the $Fe_{75}Al_{25}$ mechanically alloyed powders reported in Fig. 2. In this case the rapid diffusion of aluminium into the b c c α-iron lattice is accomplished soon after 1 h, with the formation of an Fe(Al) extended solid solution, showing just a weak trace of the Al(1 1 1) peak. Note also the use of the logarithmic scale which underlines the weaker features of the pattern. The positions of the peak maxima and the lattice parameters of the $Fe_{75}Al_{25}$ MA alloys are reported in Table I. Initially the lattice parameter of the b c c phase remains constant, even after the disappearance from the pattern of the peaks of aluminium. An analogous disappearance of silicon peaks as a function of the MA time was reported in recent works on the $W_{76}Si_{24}$ [26] and on the $Pd_{75}Si_{25}$ [27] systems. Because even in those cases the lattice parameter of the major constituent phase was not correlated with the disappearance of the silicon peaks, it was suggested that small crystallites (< 20 nm) of silicon are transparent to X-rays. We have rejected the hypothesis of aluminium transparency in our $Fe_{75}Al_{25}$ MA specimen, because a mechanical mixture of iron and aluminium ball-milled separately does show intense peaks of f c c Al, that is, the absorption of X-rays is governed by the amount of a substance, not by its average crystallite size. Thus, in the X-ray pattern of the specimen MA for 2 h, we

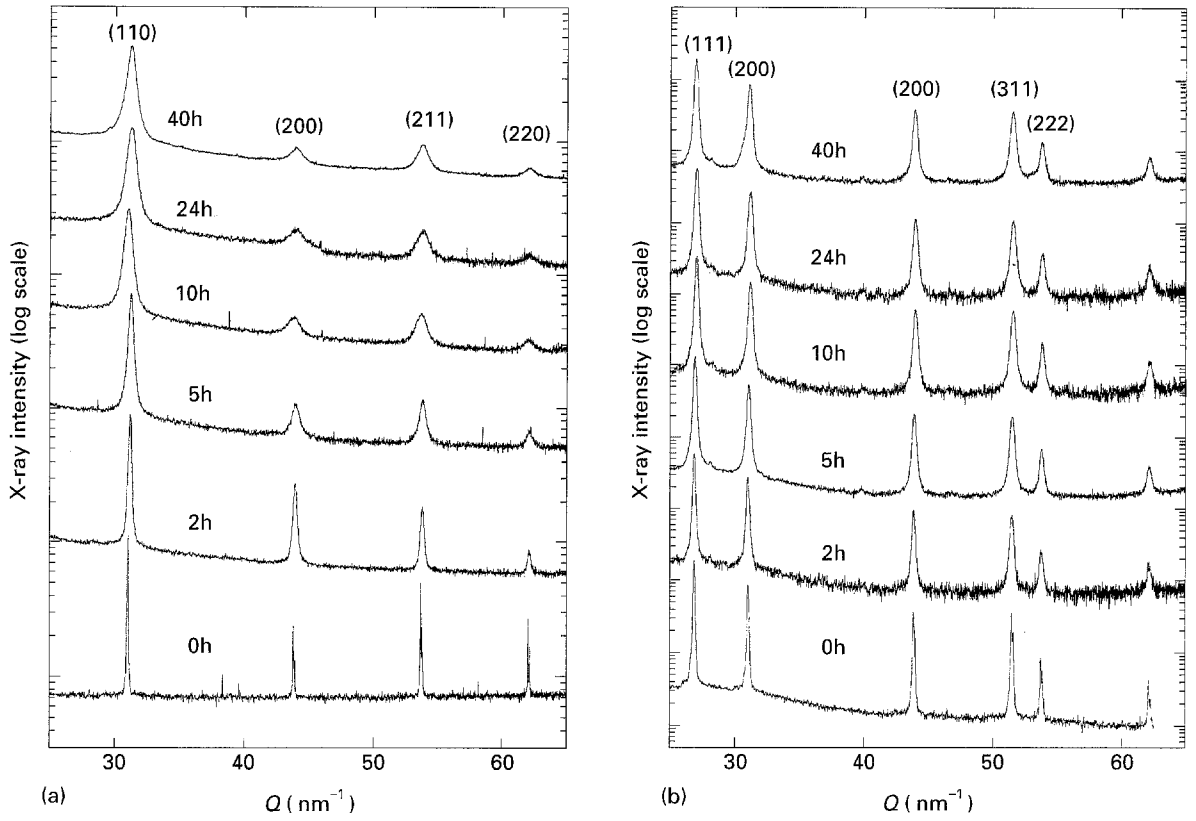

Figure 1 (a) Logarithmic XRD intensity versus scattering vector Q of α-iron powders milled for the times indicated; (b) same graphs for the aluminium powders.

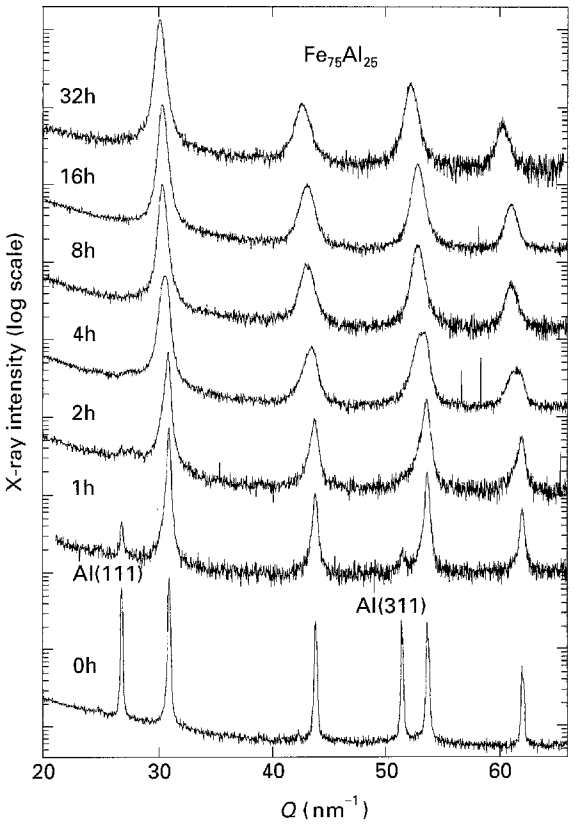

Figure 2 XRD intensity versus scattering vector Q for the $Fe_{75}Al_{25}$ elemental powders milled for the times indicated. Note the disappearance of the Al(1 1 1), Al(3 1 1) peaks soon after 1 h milling, with formation of a b c c solid solution.

observe just a single, nanostructured, b c c phase. The peaks of the specimens MA 1, 2 and 4 h are strongly asymmetrical in shape, with a skeweness to low-Q which is beyond any instrumental effect of the diffractometer. In Table I, a significant modification of the lattice parameter of the solid solution can be evaluated only after 4 h MA, and for times longer than 8 h no further changes are observed. Also in the Fe–Al powders obtained by mechanical milling of melt-spun ingots, the formation of b c c, iron-based, solid solution was reported. The lattice parameter of the b c c phase was found to increase linearly with aluminium content up to 25 at % [21].

By means of the procedure of line broadening analysis discussed previously it is possible to separate quantitatively the strain level, $\langle \varepsilon^2 \rangle^{1/2}$, and the effective crystallite size, $\langle D \rangle$, using the (1 1 0) and (2 2 0) couple of reflections. Figs. 3a and b show the average crystallite size $\langle D \rangle$, and the average strain, $\langle \varepsilon^2 \rangle^{1/2}$, as a function of the milling time for pure iron, aluminium and for the Fe–Al binary case. The data for iron are in agreement with those reported by Wagner and Boldrick [11], while those of aluminium confirm the data of Eckert *et al.* [7]. This analysis shows that the extended milling affects the formation of nanocrystalline phases. The trend of the grain size and of the lattice disorder with milling time for the $Fe_{75}Al_{25}$ composition is between the curves traced for pure aluminium and iron, but closer to that of iron. Transmission electron micrographs of the $Fe_{75}Al_{25}$ alloys MA 4 and 16 h reported in Figs 4a and b, respectively, confirm the range of sizes obtained from the X-ray diffraction line broadening. Although the process of refinement of the microstructure is qualitatively the same, a significant difference between iron and aluminium is observed in the ultimate grain size of Fig. 3a and in the atomic level strain of Fig. 3b. This result is in agreement with the observed scaling of the ultimate

TABLE I Results of the profile fitting analysis adopted to evaluate the position and broadening of the X-ray peaks

MA time		*hkl* reflections 110	200	211	220	a_0(nm)
0 h	Q_0(nm^{-1})	30.97	43.83	53.66	61.97	0.2868
	β(nm^{-1})	00.18	00.17	00.15	00.18	
	w_1(nm^{-1})	00.058	00.051	00.062	00.079	
1 h	Q_0(nm^{-1})	30.94	43.81	53.67	61.98	0.2867
	β(nm^{-1})	00.43	00.63	00.54	00.53	
	w_1(nm^{-1})	00.12	00.18	00.14	00.14	
2 h	Q_0(nm^{-1})	30.94	43.80	53.65	61.99	0.2867
	β(nm^{-1})	00.58	00.90	00.88	00.93	
	w_1(nm^{-1})	00.12	00.22	00.18	00.19	
4 h*	Q_0(nm^{-1})	30.80	43.58	53.37	61.61	0.2885
	w_1(nm^{-1})	00.31	00.43	00.44	00.56	
8 h	Q_0(nm^{-1})	30.54	43.15	52.86	61.03	0.2912
	β(nm^{-1})	00.76	01.55	00.92	01.41	
	w_1(nm^{-1})	00.289	00.589	00.492	00.564	
16 h	Q_0(nm^{-1})	30.49	43.18	52.86	61.05	0.2911
	β(nm^{-1})	00.78	01.69	01.27	01.42	
	w_1(nm^{-1})	00.30	00.56	00.48	00.538	
32 h	Q_0(nm^{-1})	30.57	43.16	52.61	60.92	0.2915
	β(nm^{-1})	00.87	01.78	01.39	01.59	
	w_1(nm^{-1})	00.33	00.66	00.54	00.58	

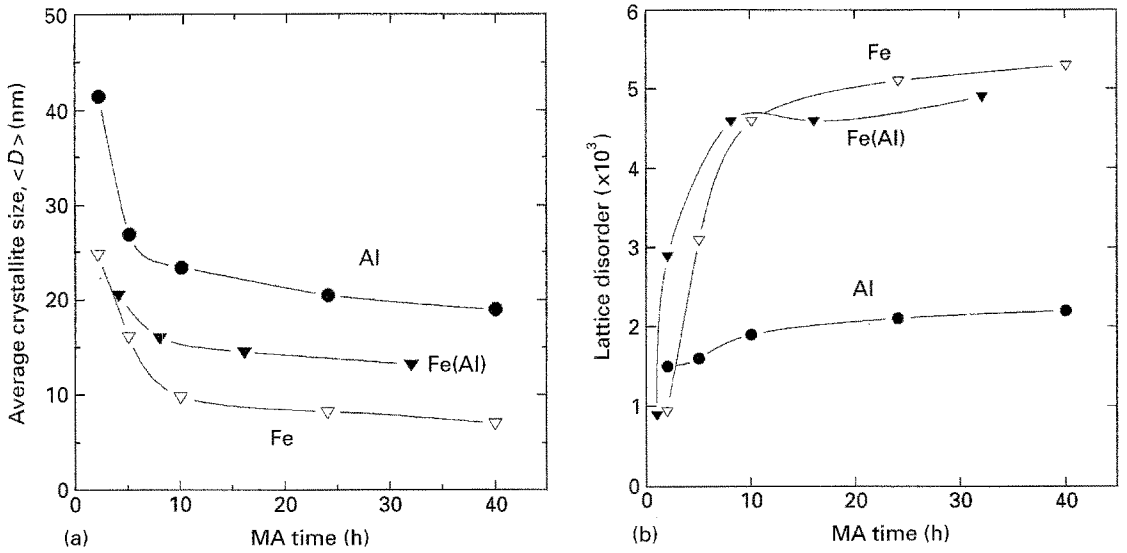

Figure 3 (a) Average crystallite size for pure iron, aluminium and for the $Fe_{75}Al_{25}$ mixture, as a function of the milling time; (b) root mean square strain $\langle\varepsilon^2\rangle^{1/2}$ for the iron, aluminium and $Fe_{75}Al_{25}$ powders milled for the times indicated.

grain size, $\langle D\rangle$, with the melting point or with the bulk moduli of nanocrystalline pure metals prepared by mechanical alloying [5]. The ultimate grain size reached during the mechanical attrition is determined by the equilibrium between the mechanical deformation due to dislocations and the recovery rate [5]. It has been reported that in the absence of recovery, assuming the validity of a dislocation pile-up model for slip, the lower limiting value of the grain size is determined by the critical dislocation distance, L, in a pile-up, that can be expressed as:

$$L = 3Gb/\pi(1-\nu)h \quad (6)$$

where G is the shear modulus, b the modulus of the Burgers vector (in practice the nearest neighbour distance), ν Poisson's ratio and h the hardness of the material [28]. In addition, Eckert *et al.* [5] have reported that the average crystallite size, $\langle D\rangle$, obtained by ball milling in a number of pure metals, is two to three times larger than L due to a competition between the effect of mechanical deformation and the rate of recovery.

In the case of solid solutions, an increase of the hardness is expected, thus reducing the ultimate grain size, L, in Equation 3. This fact has been confirmed in the case of fcc Cu–Fe supersaturated extended solutions, where the ultimate grain size was found to depend inversely on the solute content [5]. However the same approach failed to describe the behaviour of bcc Fe–Cu alloys produced by MA and this was

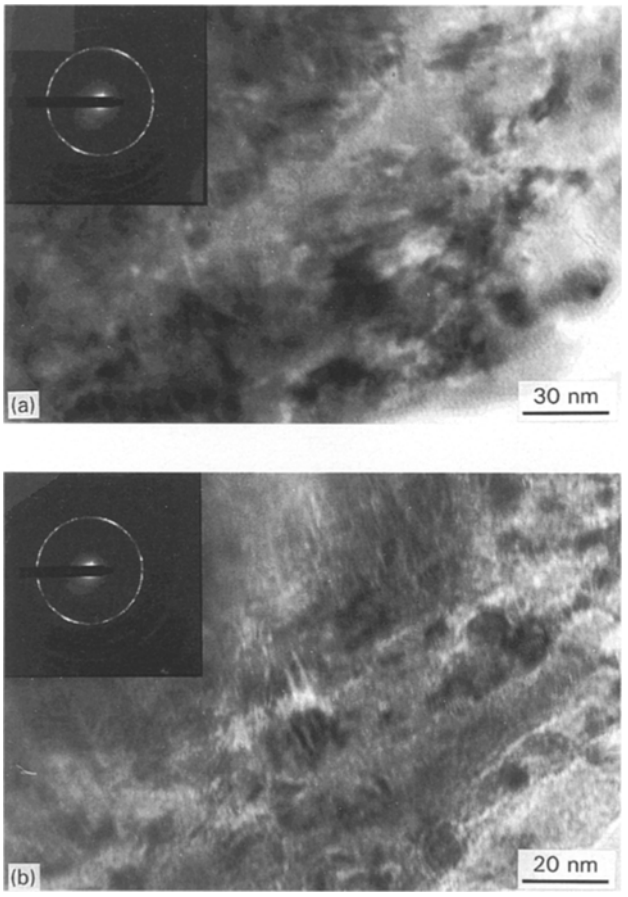

Figure 4 (a) TEM bright-field image of the $Fe_{75}Al_{25}$ powder milled 4 h; (b) TEM bright-field image of $Fe_{75}Al_{25}$ alloys milled 32 h. A nanostructured b c c phase with grains in the size range 10–20 nm can be observed in both pictures. Inset: the corresponding diffraction pattern.

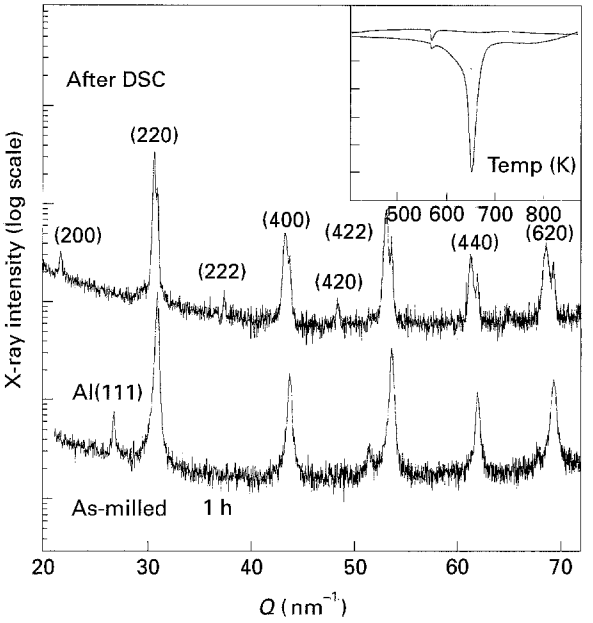

Figure 5 XRD spectrum of the Fe(Al) solid solution after 1 h MA subjected to the DSC run shown in the inset. The strong exothermic peak is related to the transformation of the powder to Fe_3Al.

ascribed to stabilization and locking of normally unstable stacking faults. In the Fe–Cu system, a similarity of atomic size of the constituent atoms rules out the elastic locking of stacking faults, which conversely, should be operative in the present Fe–Al system. G, ν and h of the Fe–Al solid solution are obtained from the pure constituents after assuming that these properties depend linearly on the composition (Vegard-like approximation). This assumption leads to an ultimate grain size $L \simeq 4.2$ nm, which, as with the pure elements, scales by a factor of 3 with the experimental value $\langle D \rangle$ of 13 nm obtained from X-ray diffraction. Moreover it should be noted that our results refer to a b c c solid solution and to a binary system which is reported miscible in the equilibrium phase diagram, whilst Eckert *et al.* [5, 29] have developed this approach for the Cu–Fe immiscible system. Of course, other Fe–Al compositions should be studied in order to assess the applicability of this approach, and these experiments are in progress.

The transformation from the single-phase Fe(Al) solid solution to a nanostructured Fe_3Al intermetallic can be observed in the DSC trace up to 873 K, shown in the inset of Fig. 5 and referred to the specimen MA for 1 h. In fact, from the XRD pattern of the powder after the DSC of Fig. 5, a peak shift analysis allows calculation of a lattice parameter $a_0 = 0.5795(2)$ nm, which is close to the value of 0.578 nm reported for the Fe_3Al intermetallic. In addition, some untransformed α-iron or Fe(Al) solid solution with the lattice parameter unchanged seems to be still present, as suggested by evident splitting of the b c c sequence of peaks in Fig. 5. Furthermore, we have found that the transformation temperature depends weakly on the average grain size of the Fe(Al) solid solution.

The elastic energy dissipation coefficient, Q^{-1}, versus temperature during the first thermal run of the specimen MA 1 h shows a wide peak whose nature is intrinsically structural and not relaxational, and is accompanied by a significant modulus increase in the temperature range 550–650 K (Fig. 6a). In the second thermal run of Fig. 6b, the modulus of the specimen MA 1 h displays a smooth decreasing trend reflecting an isoconfigurational temperature dependence due essentially to anharmonicity effects of the microstructure. According to the results of Fig. 5 and to our previous study [30], this microstructure consists of a mixture of the Fe_3Al compound and of the Fe(Al) b c c solid solution.

The specimens milled for 16 h give rise to a completely different anelastic spectrum. The background damping at room temperature before the first thermal run is somewhat lower than in the specimens milled for lower times. This result conforms to a general behaviour, observed also on pure metals, and should reflect a reduction in the defect density [31]. Moreover, the damping behaviour in the temperature range 550–650 K, where the transformation from the nanophase Fe(Al) solid solution to the disordered Fe_3Al intermetallic occurs, involves very low amounts of dissipated elastic energy, also revealed in the corresponding smooth increase of the modulus.

Fig. 7a shows the isothermal (623 K) moduli of specimens milled for, 2, 16 and 32 h, and shows that the relative variation of the dynamic Young's modulus decrease as a function of the milling time. This can be

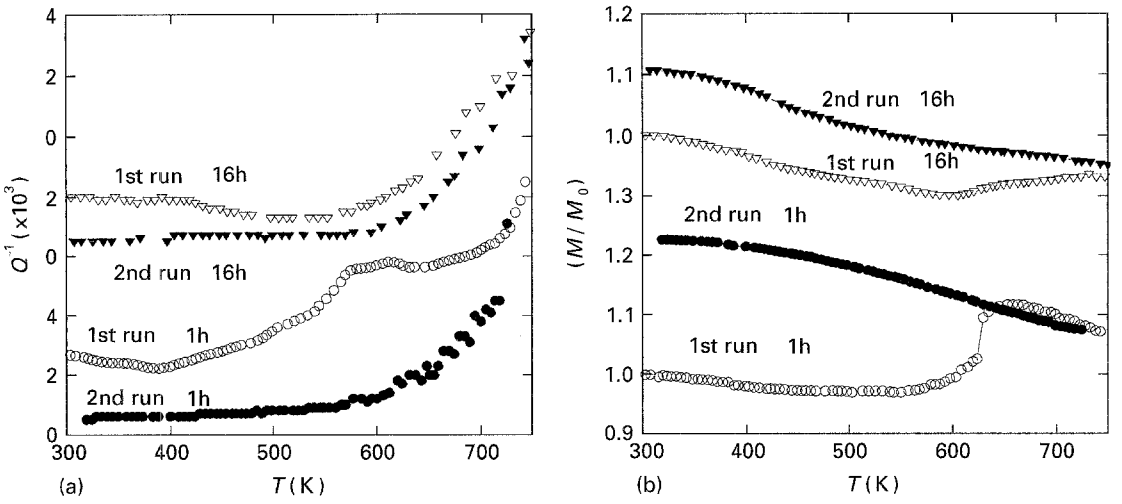

Figure 6 (a) Elastic energy dissipation coefficient, Q^{-1} (internal friction) versus temperature for specimens milled (○, ●) 1 h and (△, ▲) 16 h in the (○, △) first and (●, ▲) second thermal runs. Note the wide structural peak in the first run of the specimen milled for 1 h. (b) Corresponding dynamic Young's modulus versus temperature curve. The values are normalized to their values M_0 at room temperature at the beginning of the first run. Vibration frequency 600 Hz.

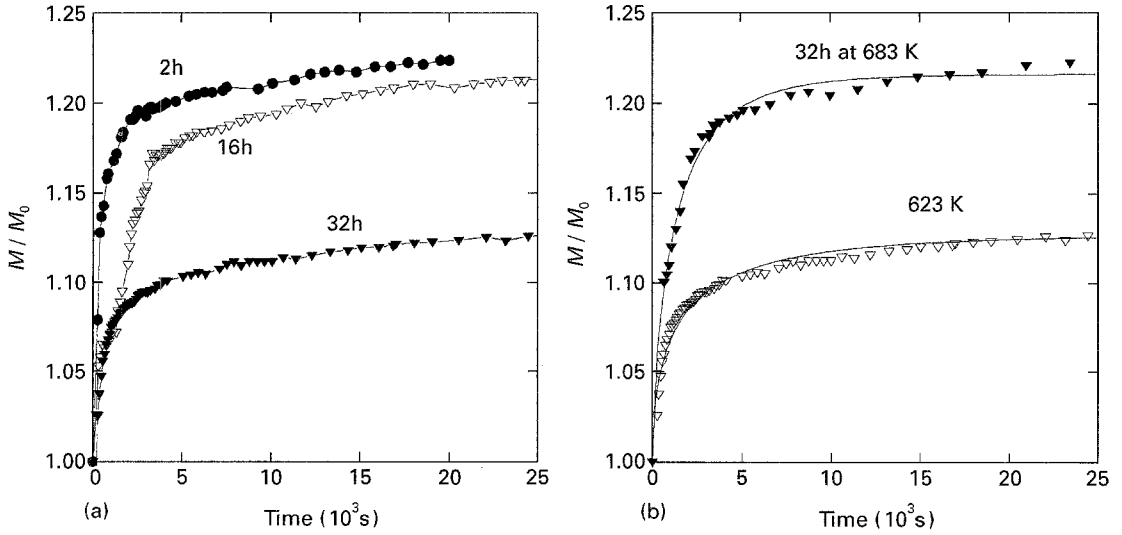

Figure 7 (a) Comparison of the dynamic Young's modulus, M, of specimens milled for different times during isothermal measurement at 623 K. (b) Dynamic Young's modulus trends during two isothermal measurements at the indicated temperatures on the $Fe_{75}Al_{25}$ specimens milled for 32 h.

related to the amount of dissipated energy. In addition, the different trend of the moduli of samples milled 32 h at 623 and 683 K (Fig. 7b), suggests again a definite temperature for the structural transformation. This transformation was also characterized in detail elsewhere by XRD, TEM and EDS analyses [30, 32]. Quantitative fits of the isothermal modulus have been performed on the basis of a Johnson–Mehl–Avrami type equation (solid lines in Fig. 7b)

$$M/M_0 = 1 + \Delta M\{1 - \exp[-(at)^n]\} \quad (7)$$

with ΔM, a and n adjustable parameters. The refined value of $n \simeq 0.7$ is related to the ascending trend of the curves at long times of treatment, and this makes it difficult to single out a precise physical meaning for this parameter. However, it is interesting to point out a value of the activation energy of $1.8(\pm 0.5)$ eV, which is close to 1.73 eV reported for the interdiffusion of aluminium into the Fe(Al) disordered phase using electron microprobe analysis [33]. Of course these data require deeper evaluation, and further work, supplemented by DSC analyses, is in progress to investigate the thermally activated transformations of the Fe–Al system alloyed with different mechanical treatments and with controlled addition of extra elements.

4. Conclusion

The X-ray diffraction results of pure iron and aluminium and of a mixture of $Fe_{75}Al_{25}$ subjected to high-energy ball milling indicate the existence of an intrinsic limit of the grain size, $\langle D \rangle$. This is ~ 70, ~ 200 and ~ 130 nm for iron, aluminium and the Fe(Al) solid solution, respectively. The $\langle D \rangle$ value of the binary alloy falls within the critical length scale accepted for the application of a simple model for polycrystal slip and plasticity, based on the pile-up of dislocations. A moderate thermal ageing makes the solid solution transform into a disordered Fe_3Al intermetallic at a definite temperature $T \sim 650$ K. Anelasticity

measurements in mechanically alloyed and thermally aged specimens confirmed that the free energy content of the metastable state obtained after long mechanical alloying time is close to the intermetallic nanophase. In addition, the reduction of the background damping at low temperature as a function of milling time suggests a reduction of the defect density in the ultimate grain size.

Acknowledgements

The authors thank the National Institution for the Physics of Matter (INFM) and MURST (Italy) for financial support, Professor G. Cocco for useful discussions and for providing, the powdered specimens, and also the Centro Sperimentale Metallurgico (Rome) for their interest in the research.

References

1. C. POLITIS and W. L. JOHNSON *J. Appl. Phys.* **60**, (1986) 1147.
2. A. E. YERMAKOV, E. E. YURCHIKOV and V. A. BARINOV, *Fiz. Met. Metallov.* **52** (1981) 1184.
3. E. HELLSTERN and L. SCHULTZ, Philos. Mag. *B* **56** (1987) 443.
4. H. J. FECHT, E. HELLSTERN, Z. FU and W. L. JOHNSON, *Metall. Trans.* **21A** (1990) 2333.
5. J. ECKERT, J. C. HOLZER, C. E. KRILL and W. L. JOHNSON, *J. Mater. Res.* **7** (1992) 1751.
6. E. BONETTI, G. VALDRÈ, S. ENZO and G. COCCO, *J. Alloys Compounds* **194** (1993) 331.
7. J. ECKERT, J. C. HOLZER, C. E. KRILL´III and W. L. JOHNSON, *Mater. Sci. Forum.* **88–90** (1992) 505.
8. G. COCCO, S. ENZO, L. SCHIFFINI and L. BATTEZZATTI, *Mater. Sci. Eng.* **97** (1988) 34.
9. S. ENZO, E. BONETTI, I. SOLETTA and G. COCCO, *J. Phys. D. Appl. Phys.* **24** (1991) 209.
10. E. GAFFET and M. HARMELIN, *J. Less-Common Metals* **157** (1990) 201.
11. C. N. J. WAGNER and M. S. BOLDRICK, *Mater. Sci. Eng.* **A133** (1991) 26.
12. H. BAKKER and L. M. DI, *Mater. Sci. Forum* **88–90** (1992) 27.
13. R. B. SCHWARZ and C. C. KOCH, *Appl. Phys. Lett.* **49** (1986) 148.
14. A. CALKA, *Key Engn. Mater.* **81–83** (1993) 17.
15. X. ZHU, R. BIRRINGER, U. HERR and H. GLEITER, *Phys. Rev.* **B35** (1987) 9085.
16. J. RUPP and R. BIRRINGER, *ibid.* **B36** (1987) 7888.
17. M. R. FITZIMMONS, J. A. EASTMAN, M. MULLER-STACH and G. WALLNER, *ibid.* **B44** (1991) 2452.
18. M. A. MORRIS and D. G. MORRIS, *Mater. Sci. Forum* **88–90** (1992) 529.
19. Y. D. DONG, W. H. HUANG, L. LIU, K. Q. XIAO, S. H. TONG and Y. Z. HE, *Mater. Sci. Eng. A* **134** (1991) 867.
20. T. ZAK, O. SCHNEIWEISS, Z. COCHNAR and A. BUCHAL, *ibid.* **A141** (1991) 73.
21. E. P. YELSUKOV, E. V. VORONINA and V. A. BARINOV, *J. Mag. Magn. Mater.* **115** (1992) 271.
22. N. BURGIO, A. IASONNA, M. MAGINI, S. MARTELLI and F. PADELLA, *Nuova Cimento* **13** (1991) 459.
23. S. ENZO, S. POLIZZI and A. BENEDETTI, *Z. Kristall.* **170** (1985) 275.
24. A. GUINIER, "X-ray diffraction", (Freeman, San Francisco, CA, 1963).
25. C. N. J. WAGNER, *Adv. X-ray Anal.* **7** (1964) 46.
26. B. BOKHONOV, E. IVANOV and V. BOLDYREV, *J. Alloys Compounds* **199** (1993) 125.
27. M. MAGINI, N. BURGIO, S. MARTELLI, F. PADELLA, E. PARADISO and G. ENNAS, *J. Mater. Sci.* **26** (1991) 3969.
28. T. G. NIEH and J. WADSWORTH, *Scripta Metall Mater.* **25** (1991) 955.
29. J. ECKERT, J. C. HOLZER, C. E. KRILL and W. L. JOHNSON, *J. Appl. Phys.* **73** (1993) 2794.
30. E. BONETTI, G. SCIPIONE, G. VALDRÈ, G. COCCO, R. FRATTINI and P. P. MACRÌ, *ibid.* **74** (1993) 2053.
31. E. BONETTI and G. VALDRÈ, *Philos. Mag. B* **68** (1993) 967.
32. E. BONETTI, G. VALDRÈ, S. ENZO, G. COCCO and I. SOLETTA, *Nanostruct. Mater.* **2** (1993).
33. "Diffusion Data", Vol. 3. nos. 1–3 edited by F. H. Wohlbier (Diffusion Information Center, Cleveland, OH (1969) p. 270.

Received 17 May
and accepted 21 September 1994